Über die analytische Fortsetzung von Greenschen Funktionen in der Vielteilchenphysik

Philipp Kaufmann

München 2023

Über die analytische Fortsetzung von Greenschen Funktionen in der Vielteilchenphysik

Philipp Kaufmann

Bachelorarbeit
Lehrstuhl für theoretische Festkörperphysik
Fakultät für Physik
Ludwig–Maximilians–Universität
München

vorgelegt von
Philipp Kaufmann
aus München

München, den 24.07.2023

Betreuer: Jan von Delft

On the Analytic Continuation of Green Functions in Many-Body Physics

Philipp Kaufmann

Munich 2023

On the Analytic Continuation of Green Functions in Many-Body Physics

Philipp Kaufmann

Bachelor thesis
chair of theoretical solid state physics
faculty of physics
Ludwig–Maximilians–Universität
Munich

submitted by
Philipp Kaufmann
from Munich

Munich, 24.07.2023

Supervisor: Jan von Delft

Contents

Abstract

Calculations for finite-temperature Green functions in many-body physics are usually done in the Matsubara formalism through which imaginary time results are generated. The real time Green function can be obtained from these results by analytic continuation. However, this analytic continuation problem is ill-conditioned numerically and turns out to be a difficult task. A number of different approaches have been developed in recent years. They show different behavior in terms of accuracy, performance, numerical stability, and sensitivity to noisy input data. In this thesis, I want to compare the well-established Padé approximation with two recently proposed methods, namely PES and Nevanlinna. These two methods guarantee the non-negativity constraint of the spectral function per construction. This is a common problem of Padé approximation. In addition, I show that Padé approximation can be improved by using the AAA algorithm for interpolation.
These methods are applied to data for Matsubara Green functions that correspond to the Anderson impurity model, a spectral function composed of Gauss functions, and a spectral function corresponding to a finite-energy system.

Chapter 1

Introduction

Condensed matter physics is the branch of physics that deals with the properties of liquid and solid substances. The discovery of quantum mechanics around 1920 led to great advances in the field. Notable examples are Pauli's theory of paramagnetism and Sommerfeld's free-electron model which predicts the temperature dependence of the heat capacity of metals. Also, the theory of electronic band structure is rooted in quantum mechanics which can explain the conductive properties of metals, insulators, or semiconductors. Today, life without digital devices such as smartphones or computers is hard to imagine. Such technologies wouldn't be available without the human understanding of semiconductors.

Despite this huge success, some properties of condensed matter remained without theoretical explanation using only quantum mechanics. Phenomena such as superconductivity or the Kondo effect called for new approaches to the description of matter. This was eventually done by using new ideas which were originally developed in quantum field theory for quantum many-body systems. This way in 1957 the BCS theory for superconductivity was developed, providing a quantum many-body model for the behavior of conventional superconductors.

A common problem in many-body physics is the analytic continuation of Green functions. In 1.1, I give an introduction to this problem. In 2, I explain the mechanism of Padé approximation and the two recently proposed Nevanlinna and PES methods that were developed for this problem. I also show how Padé approximation can be modified using the AAA algorithm for rational approximation. In 3, the performance of all of the introduced methods is compared for various input data. Finally, in 4, a summary of the results as well as some ideas about how this problem can be approached in the future is given.

1.1 The analytic continuation problem

1.1.1 Green functions for solving differential equations

Green functions are a powerful tool for solving linear differential equations. A standard example that illustrates the mechanism of Green functions is finding a solution for the Poisson equation:

$$\triangle\phi(\vec{r}) = -\frac{1}{\epsilon_0}\rho(\vec{r}) \tag{1.1}$$

The equation relates the electric potential ϕ to the charge carrier density ρ. $\triangle$ is the Laplace operator. The Green function is defined as the function which yields a delta function when the differential operator of the differential equation is applied to it:

$$\triangle G(\vec{r}) = \delta(\vec{r}) \tag{1.2}$$

The Green function for the Laplace operator is [1]:

$$G(\vec{r}) = -\frac{1}{4\pi r} \tag{1.3}$$

Once the Green function is known, the solution for the differential equations can be obtained from the convolution of the inhomogeneous part of the differential equation and the Green function:

$$\phi(\vec{r}) = -\frac{1}{\epsilon_0}\int \mathrm{d}\vec{r}' G(\vec{r}-\vec{r}')\rho(\vec{r}') = \frac{1}{4\pi\epsilon_0}\int \mathrm{d}\vec{r}' \frac{\rho(\vec{r}')}{|\vec{r}-\vec{r}'|} \tag{1.4}$$

Green functions can be viewed as building blocks that can be used to create solutions for differential equations.

1.1.2 Green functions in many-body physics

In many-body physics, Green functions are defined in a similar way [1]. First, consider the Schrödinger equation for a single particle:[2]

$$[\mathrm{i}\partial_t - H(\vec{r})]\Psi(\vec{r},t) = 0 \tag{1.5}$$

The Green function is then defined by:

$$[\mathrm{i}\partial_t - H(\vec{r})]G(\vec{r},t;\vec{r}',t') = \delta(\vec{r}-\vec{r}')\delta(t-t') \tag{1.6}$$

We can use a Green function to describe the time evolution of a state $\Psi(\vec{r}',t')$ at time t' to time t:

$$\Psi(\vec{r},t) = \int \mathrm{d}t' \int \mathrm{d}\vec{r}' G(\vec{r},t;\vec{r}',t')\Psi(\vec{r}',t') \tag{1.7}$$

$\Psi(\vec{r},t)$ satisfies the Schrödinger equation 1.5. This can be seen by inserting 1.7 in 1.5 and using 1.6. For this reason $G(\vec{r},t;\vec{r}',t')$ is also called *propagator*.

[1] This is only a very brief introduction to Green functions and their use in many-particle physics. For a more detailed discussion see Chapters 8 and 11 in [2].

[2] $\hbar$ is set to 1 in all equations in this thesis.

Retarded Green functions

An important solution for 1.6 is the *retarded Green function.*

$$G^R(\vec{r},t;\vec{r}',t') = -\mathrm{i}\theta(t-t')\langle\vec{r}|e^{-\mathrm{i}H(t-t')}|\vec{r}'\rangle \tag{1.8}$$

It is the amplitude for the particle to be in state $|\vec{r}\rangle$ at time t, given that it was in state $|\vec{r}'\rangle$ at time t'. G^R could also be represented in another basis by replacing $\langle\vec{r}|$ and $|\vec{r}'\rangle$ with vectors of the new basis. It is often useful to express the retarded Green function in an eigenbasis of the Hamiltonian. Let $\{|\phi_n\rangle\}$ be a complete eigenbasis of H with $H|\phi_n\rangle = E_n|\phi_n\rangle$. We can then rewrite 1.8 to:

$$G^R(\vec{r},t;\vec{r}',t') = -\mathrm{i}\theta(t-t')\sum_n\langle\vec{r}|\phi_n\rangle\langle\phi_n|\vec{r}'\rangle e^{-\mathrm{i}E_n(t-t')} \tag{1.9}$$

Many-body systems

So far, we have only discussed single particles and neglected the interactions between them. In many-body physics a more general definition of the retarded Green function is needed. The retarded Green function is now rewritten in terms of annihilation/creation operators:

$$G^R_{\nu,\nu'}(t-t') = -\mathrm{i}\theta(t-t')\left\langle\left\{a_\nu(t),a^\dagger_{\nu'}(t')\right\}\right\rangle \tag{1.10}$$

$a_\nu(t)$ is the annihilation operator for a state $|\nu\rangle$ and $a^\dagger_{\nu'}(t)$ is creation operator for a state $|\nu'\rangle$. ν and ν' are quantum numbers. Both states are given in the Heisenberg picture. They are related to the Schrödinger picture operators a_ν and $a^\dagger_\nu$ by:

$$a_\nu(t) = e^{\mathrm{i}Ht}a_\nu e^{-\mathrm{i}Ht} \tag{1.11}$$

$$a^\dagger_\nu(t) = e^{\mathrm{i}Ht}a^\dagger_\nu e^{-\mathrm{i}Ht} \tag{1.12}$$

$\{\cdot,\cdot\}$ is the fermionic anticommutator:

$$\{A,B\} = AB+BA \tag{1.13}$$

$\langle ...\rangle = \frac{1}{Z}\mathrm{Tr}(e^{-\beta H})$ denotes the thermal expectation value where $\beta = \frac{1}{k_BT}$.
For simplicity, I will only discuss fermionic systems here. The treatment of bosonic systems is very similar.
Since we are considering system in thermal equilibrium, $G^R_{\nu,\nu'}(t-t')$ is a function of time difference only. We can perform a Fourier transformation to get a function in the frequency domain. Before doing that, we again express the Green function through energy eigenstates:

$$\begin{aligned}G^R_{\nu,\nu'}(t-t') = -\mathrm{i}\theta(t-t')\frac{1}{Z}\sum_{nn'}e^{-\beta E_n}\big(&\langle\phi_n|a_\nu|\phi_{n'}\rangle\langle\phi_{n'}|a^\dagger_{\nu'}|\phi_n\rangle e^{\mathrm{i}(E_n-E_{n'})(t-t')}\\ &+\langle\phi_n|a^\dagger_{\nu'}|\phi_{n'}\rangle\langle\phi_{n'}|a_\nu|\phi_n\rangle e^{-\mathrm{i}(E_n-E_{n'})(t-t')}\big)\end{aligned} \tag{1.14}$$

The Fourier transformation of $G^R_{\nu,\nu'}(t-t')$ is:

$$\begin{aligned} G^R_{\nu,\nu'}(\omega+i\eta) &= \int_{-\infty}^{\infty} \mathrm{d}t e^{\mathrm{i}(\omega+\mathrm{i}\eta)t} G^R_{\nu,\nu'}(t) \\ &= \frac{1}{Z}\sum_{nn'} \frac{\langle\phi_{n'}|a_\nu|\phi_{n'}\rangle\langle\phi_{n'}|a^\dagger_\nu|\phi_n\rangle}{\omega+E_n-E_{n'}+\mathrm{i}\eta}\left(e^{-\beta E_n}+e^{-\beta E_{n'}}\right) \end{aligned} \tag{1.15}$$

η is a positive infinitesimal number, which is necessary to ensure that the integrand converges. Eq. 1.15 is called *Lehmann representation* of $G^R_{\nu,\nu'}$.

Using the Green function in the frequency domain, the *spectral function* is defined

$$A(\omega) = \lim_{\eta\to 0} -\frac{1}{\pi}\mathrm{Im}G^R_{\nu,\nu'}(\omega+i\eta) \tag{1.16}$$

which can also be written in Lehmann representation [2],

$$A(\omega) = \frac{1}{Z}\sum_{nn'}\langle n|c_\nu|n'\rangle\langle n'|c^\dagger_\nu|n\rangle e^{-\beta E_n}(1+e^{-\beta\omega})\delta(\omega+E_n-E_{n'}) \tag{1.17}$$

It contains information about the distribution of quantum states independent of their occupation. It can be measured using, e.g., photoemission spectroscopy. A property of the spectral function is that it fulfills the sum rule

$$\int_{-\infty}^{\infty} \mathrm{d}\omega A(\omega) = 1 \tag{1.18}$$

and that A is always non-negative:

$$A(\omega) \geq 0, \forall\omega \tag{1.19}$$

1.1.3 Imaginary time Green functions

When dealing with systems at finite-temperature, one would expect that things will become very difficult because now we need to consider quantum effects over a large ensemble of possible states whose probability is given by the Boltzmann distribution: $p_i = \frac{e^{-\beta E_i}}{Z}$, where $\beta = \frac{1}{k_B T}$. However, in practice, working with finite-temperature systems is often not more difficult than with zero-temperature systems. This is because the concept of *imaginary time* can be used. To get an idea of why the imaginary time formalism works, one can consider the inverse temperature β as the imaginary time in a time evolution operator. It shows a lot of calculations are done more practicable in this formalism. Therefore, most finite-temperature calculations for the Green function are done using imaginary time. Then, analytic continuation is used to obtain the real time function.

To work with imaginary time, we replace the real time t with an imaginary valued expression $t \to -\mathrm{i}\tau$, where τ is a real number. For example, operators in the Heisenberg picture then become:

$$A(t) = e^{itH} A e^{-itH}$$
$$\downarrow$$
$$A(\tau) = e^{\tau H} A e^{-\tau H}$$

The *imaginary time* or *Matsubara Green function* is defined:

$$\mathcal{C}_{\nu\nu'}(\tau - \tau') = -\left\langle T_\tau a_\nu(\tau) a^\dagger_{\nu'}(\tau') \right\rangle \tag{1.20}$$

Still, we are only considering fermionic systems. T_τ is the imaginary time-ordering operator. It orders operators such that operators with a later time appear on the left while respecting the anticommuting behavior of fermionic creation/annihilation operators:

$$T_\tau \left(A(\tau)B(\tau')\right) = \theta(\tau - \tau')A(\tau)B(\tau') - \theta(\tau' - \tau)B(\tau')A(\tau) \tag{1.21}$$

Again, $\mathcal{C}_{\nu\nu'}$ is a function of time difference only. It can be proven that $\mathcal{C}_{AB}$ is well-defined only for $-\beta < \tau - \tau' < \beta$ and it is antiperiodic $\mathcal{C}_{AB}(\tau) = -\mathcal{C}_{AB}(\tau + \beta)$ [3]. Thus, the function can be expressed as a Fourier series:

$$\begin{aligned}
\mathcal{C}_{\nu\nu'}(\tau) &= \frac{1}{\beta} \sum_{n=-\infty}^{\infty} e^{-i\pi n\tau/\beta} \mathcal{C}_{\nu\nu'}(n) \\
\mathcal{C}_{\nu\nu'}(n) &= \frac{1}{2} \int_{-\beta}^{\beta} \mathrm{d}\tau e^{i\pi n\tau/\beta} \mathcal{C}_{\nu\nu'}(\tau) \\
&= \frac{1}{2}(1 - e^{-\mathrm{i}\pi n}) \int_0^\beta \mathrm{d}\tau e^{\mathrm{i}\pi n\tau/\beta} \mathcal{C}_{\nu\nu'}(\tau)
\end{aligned}$$

$\mathcal{C}_{\nu\nu'}(n)$ is only non-zero when n is odd. Using the *Matsubara frequencies* $\omega_n = \frac{(2n+1)\pi}{\beta}$ for fermionic systems, these two equations can be rewritten to:

$$\begin{aligned}
\mathcal{C}_{\nu\nu'}(\tau) &= \frac{1}{\beta} \sum_{n=-\infty}^{\infty} e^{-\mathrm{i}\omega_n\tau} \mathcal{C}_{\nu\nu'}(n) \\
\mathcal{C}_{\nu\nu'}(\mathrm{i}\omega_n) &= \int_0^\beta \mathrm{d}\tau e^{\mathrm{i}\omega_n\tau} \mathcal{C}_{\nu\nu'}(\tau)
\end{aligned}$$

To see the connection between $\mathcal{C}_{\nu\nu'}(i\omega_n)$ and the retarded Greens function $G^R_{\nu\nu'}(\omega)$ we compare the Lehmann representations of the two:

$$\mathcal{C}_{\nu\nu'}(i\omega_n) = \frac{1}{Z} \sum_{nn'} \frac{\langle n|c_\nu|n'\rangle\langle n'|c^\dagger_{\nu'}|n\rangle}{i\omega_n + E_n - E_{n'}} \left(e^{-\beta E_n} + e^{-\beta E_{n'}}\right) \tag{1.22}$$

$$G^R_{\nu\nu'}(\omega + i\eta) = \frac{1}{Z} \sum_{nn'} \frac{\langle n|c_\nu|n'\rangle\langle n'|c^\dagger_{\nu'}|n\rangle}{\omega + E_n - E_{n'} + i\eta} \left(e^{-\beta E_n} + e^{-\beta E_{n'}}\right) \tag{1.23}$$

The two functions coincide, except for the part in the denominator. We can rewrite this as just $G(z)$ where z is a complex number and note that the Matsubara function and the retarded Green function are identified by the limits $z \rightarrow i\omega_n$ and $z \rightarrow \omega + i\eta$, respectively. Indeed, the retarded Green function is obtained uniquely from the analytic continuation of the Matsubara function at all Matsubara frequencies:

$$G^R_{\nu\nu'}(\omega) = \mathcal{C}_{\nu\nu'}(\mathrm{i}\omega_n \rightarrow \omega + \mathrm{i}\eta) \tag{1.24}$$

This was formally proven by Mermin and Baym in 1960 [4]. For calculating the retarded Green function numerically, this is not well-defined, though, because the Matsubara Green function can only be known for a finite set of points. Instead, the analytic continuation has to be performed numerically. In practice, the analytic continuation procedure turns out to be a difficult problem. To illustrate this, we look at the following relation between $G(z)$ and the spectral function $A(\omega)$ [5]:

$$G(z) = \int_{-\infty}^{\infty} \mathrm{d}\omega \frac{A(\omega)}{z - \omega} \tag{1.25}$$

For large $|\omega|$, a small noise in $G(z)$ leads to a big change in $A(\omega)$, making the problem very sensitive to noise.

We can try to perform the analytic continuation straightforward, by rewriting equation 1.25 to

$$G(z) = \int_{-\infty}^{\infty} \mathrm{d}\omega K(z, \omega) A(\omega) \tag{1.26}$$

$$K(z, \omega) = \frac{1}{z - \omega} \tag{1.27}$$

and discretizing this integral to a matrix-vector multiplication:

$$\boldsymbol{G} = K\boldsymbol{A} \tag{1.28}$$

$$\boldsymbol{A} = K^{-1}\boldsymbol{G} \tag{1.29}$$

We can test this approach by generating an arbitrary spectral function $A(\omega)$ and then calculate $G(\mathrm{i}\omega_n)$ for a set of frequencies using 1.25. Then, we use 1.29 to get back $A(\omega)$, which should be exactly the same as before. We would see that this does not work at all - even for the most basic spectral functions the data we would get back for $A(\omega)$ looks like random noise. The reason for this is that K is ill-conditioned. The singular values of K lie in an extremely wide range [6]. The condition number of a K which indicates how well K can be inverted numerically is given by the ratio of the biggest and smallest singular value. Thus, for K the condition number is extremely big, meaning that inverting the matrix numerically without big errors is impossible. Because of that, we need to look at some more sophisticated approaches for the analytical continuation.

1.2 The Anderson impurity model

Before doing this, I want to give an example of a physical system to which the discussed tools can be applied. The *single impurity Anderson model*(SIAM) is a simple model aimed to explain the behavior of magnetic impurities in metals. These occur when small amounts of magnetic ions such as iron are added to a metallic host material. These impurity atoms may or may not form local magnetic moments. Magnetic impurities can be used to explain, for example, the Kondo effect. The Kondo effect describes the observation that for some metals below a certain temperature, the resistivity starts to rise as the temperature is lowered further. Naturally, one would expect the opposite to happen.

The Anderson model combines two ideas: 1.) Because of Coulomb interaction the d-orbitals of the impurity are strongly localized. 2) Despite their strong localization, the impurities hybridize with the host metal: The electrons can still tunnel from the orbitals to the host metal. It is sufficient to only consider a single impurity atom. The Hamiltonian of a single impurity is given by the three parts: $H = H_{bath} + H_{loc} + H_{hyb}$

$$H_{bath} = \sum_{k\sigma} \epsilon_k n_{k\sigma} \tag{1.30}$$

$$H_{loc} = \sum_{\sigma} E_d n_{d\sigma} + U n_{d\uparrow} n_{d\downarrow} \tag{1.31}$$

$$H_{hyp} = \sum_{k\sigma} v_k (c^\dagger_{k\sigma} d_\sigma + d^\dagger_\sigma c_{k\sigma}) \tag{1.32}$$

H_{bath} describes the energy of particles in the conducting sea. $n_{ks} = c^\dagger_{ks} c_{ks}$ is the number operator for the sea electron with momentum k and spin $\sigma \in \{\uparrow, \downarrow\}$. H_{loc} describes the energy of the impurity site with energy E_d. $n_{d\sigma} = d^\dagger_\sigma d_\sigma$ is the number operator for the electron at the impurity site with spin σ. If two electrons occupy the impurity they experience a repulsion U due to Coulomb interaction. Finally, H_{hyb} describes the hybridization between site electrons and sea electrons. Electrons can tunnel back and forth from the sea to the site. In this process, the tunneling constant v_k depends on the momentum k of the sea electron. Because of the hybridization, the spectrum of the localized site is broadened to the width Δ, which becomes a constant in the limit of an infinitely wide density of states for the sea electrons, considered here.

The spectral function as well as the Matsubara Green function for this model can be calculated using the *numerical renormalization group* (NRG) [7]. The energy of the impurity site is set to $E_d = -\frac{U}{2}$, corresponding to half-filling. The temperature is always set to $T = \frac{U}{100}$. In the following, I will use the NRG data for the Green function to test different methods for analytic continuation and compare the resulting spectral functions to the numerically exact one.

Chapter 2

Methods

Here, I explain the mechanisms of the methods that are tested later. I first introduce Padé approximation because it is one of the oldest and most popular methods for analytic continuation. Then, I will explain the two new methods Nevanlinna and PES which aim to improve current analytic continuation methods by enforcing the positivity constraint of the spectral function. I also show how AAA can be used as an alternative to Padé approximation.

2.1 Rational approximation

A rational function can be used to interpolate the Green function for a given set of Matsubara frequencies. The function can then be evaluated at $\omega + \mathrm{i}0^+$ to obtain the retarded Green function. Rational functions are suited because they can capture the existence and locations of poles in the resulting function, in contrast to, for example, polynomials. Another advantage of using rational functions is that they can be stored compactly since only a small number of coefficients is needed for that.

Since the approximation does not follow any physical constraints, the resulting spectral function does not necessarily obey the constraint that the function is positive at all frequencies.

2.1.1 Padé approximation

One of the first methods developed for the analytic continuation problem is called *Padé approximation*. It was first suggested in 1977 [8]. The coefficients for the rational function are determined by the *multipoint Padé approximants* algorithm. Usually, the Matsubara function for a subset of all Matsubara frequencies $\{\mathrm{i}\omega_n\}$ is used, because calculations would take a very long time otherwise. The quality of analytic continuation depends on that choice.

Multipoint Padé approximants

Padé approximation uses a simple algorithm for interpolating [8]. Given a function $f(z)$ whose function values are known for a set of points $f(z_i) = f_i$, $i = 1, \ldots, M$, the Padé approximation can be written as a continued fraction:

$$C_M(z) = \cfrac{a_1}{1 + \cfrac{a_2(z - z_1)}{1 + \cfrac{a_3(z - z_2)}{1 + \cdots + \cfrac{a_M(z - z_{M-1})}{1}}}} \tag{2.1}$$

where the coefficients a_i are determined recursively through the functions $g_i(z)$:

$$\begin{aligned} a_i &= g_i(z_i) \\ g_1(z_i) &= f_i \\ g_p(z) &= \frac{g_{p-1}(z_{p-1}) - g_{p-1}(z)}{(z - z_{p-1})g_{p-1}(z)},\ p \geq 2 \end{aligned} \tag{2.2}$$

2.1.2 Approximation using the AAA algorithm

In 2018, the *Antoulas-Anderson algorithm* (AAA) was introduced as a new algorithm to approximate rational functions whose values are known for a real or complex set of points [9]. In Appendix A, a description is given. A big difference to multipoint Padé approximants is that the algorithm chooses the points that are used for interpolation adaptively while still giving an approximation that includes all given points. AAA can therefore lead to a good approximation for all given data points much faster than Padé. Although the advantages of using the AAA algorithm for analytic continuation have been pointed out [10], the algorithm has yet not been used for the analytic continuation of Green functions. Later, I will show that the AAA algorithm leads to more accurate results than previous rational approximation techniques while taking only a small fraction of the time for calculations.

2.2 Nevanlinna

The Nevanlinna analytic continuation is a new approach to the analytic continuation problem that was developed in 2021 [5]. It uses Nevanlinna functions to interpolate the given imaginary-time data. The advantage of using Nevanlinna functions is that they preserve certain physical properties of the Green function by construction. To create a Nevanlinna function the Matsubara function is mapped from the upper complex half to the complex unit disc by a Möbius transformation. The points on the unit disc can then be interpolated by the Schur algorithm. The Nevanlinna function is then obtained by mapping this function back to the upper complex half by the inverse Möbius transformation.

2.2.1 Nevanlinna functions

A *Nevanlinna function* is a holomorphic function that maps the upper complex half-plane $\mathcal{C}^+ = \{z \in \mathbb{C} | \mathrm{Im} z > 0\}$ to its closure $\overline{\mathcal{C}^+}$. We call the set of all Nevanlinna function $\mathcal{N}$. Every Nevanlinna function can be written in the following representation [11]:

$$N(z) = C + Dz + \int_{\mathbb{R}} \left(\frac{1}{\lambda - 1} - \frac{\lambda}{1+\lambda^2} \right) \mathrm{d}\mu(\lambda) \tag{2.3}$$

where C is a real constant and D is a non-negative constant. μ is a Borel measure such that $\int_{\mathbb{R}} \frac{\mathrm{d}\mu(\lambda)}{1+\lambda^2} < \infty$. If we set

$$D = 0 \tag{2.4}$$

$$\mathrm{d}\mu(\lambda) = \frac{1}{Z} \sum_{n,n'} \langle n | c_\nu | n' \rangle \langle n' | c^\dagger_{\nu'} | n \rangle \left(e^{-\beta E_n} + e^{-\beta E_{n'}} \right) \delta(\lambda - E_n + E_{n'}) \tag{2.5}$$

$$C = \int_{\mathbb{R}} \frac{1}{1+\lambda^2} \mathrm{d}\mu(\lambda) \tag{2.6}$$

we can see by comparing $N(z)$ with equation 1.22 that $-G(z) = N(z)$. Thus, $-G(z)$ is a Nevanlinna function.
Also from the definition of Nevanlinna functions, it follows that:

$$A(\omega) = -\frac{1}{\pi} G(\omega + 0^+) = +\frac{1}{\pi} \mathrm{Im}(N(\omega + 0^+)) \geq 0 \tag{2.7}$$

Meaning that interpolating the Green function with Nevanlinna functions respects the condition that $A(\omega) \geq 0, \forall \omega$. This avoids the appearance of unphysical negative values in the final spectral function.

2.2.2 Interpolation

For interpolation, the Schur algorithm is used [1]. A Schur function is a holomorphic function that maps the open unit disc $\mathcal{D} = \{w \in \mathcal{C} || w| < 1\}$ to its closure $\overline{\mathcal{D}}$. We call the set

[1] The Schur algorithm does not work for all kinds of input data. The so-called Pick criterion is a necessary and sufficient condition. For more details, see Section 2.2.3 in [5]. Note that exact Matsubara functions fulfill this criterion while noise can lead the data to violate it.

which contains all Schur functions $\mathcal{S}$. $\mathcal{C}^+$ can be mapped to $\mathcal{D}$ using the bijective Möbius transformation h_ξ:

$$\begin{aligned}
&h_\xi : \mathcal{C}^+ \to \mathcal{D}\\
&w = h_\xi(z) = \frac{z-\xi}{z-\xi^*}\\
&h_\xi^{-1} : \mathcal{D} \to \mathcal{C}^+\\
&z = h_\xi^{-1}(w) = \frac{w\xi^* - \xi}{w-1}
\end{aligned}$$

Where $\xi \in \mathcal{C}^+$. The Schur algorithm constructs a Schur function for a given set of points in $\mathcal{D}$ using a continued fraction expression.
Given the data $G_n = G(i\omega_n)$ for a set of Matsubara frequencies $\{i\omega_n\}$ $n = 1, ..., M$, we aim to find the Nevanlinna function $f \in \mathcal{N}$ which satisfies

$$f(i\omega_n) = -G_n \equiv C_n \tag{2.8}$$

This problem can be modified to the problem by using the contractive Möbius transformation h_i

$$h_i \circ f(i\omega_n) = h_i(C_n) \equiv \lambda_n \tag{2.9}$$

which can be solved by the Schur algorithm since $C_n = f(i\omega_n) \in \mathcal{C}^+$ and $\lambda_n \in \mathcal{D}$.

2.2.3 Schur algorithm

Following the convention in [5], we will write Y_n instead of iω_n. It is useful to introduce another Möbius transformation g_ζ:

$$\begin{aligned}
&g_\zeta : \mathcal{D} \to \mathcal{D}\\
&w' = g_\zeta(w) = \frac{w+\zeta}{1+\zeta^* w}\\
&g_\zeta^{-1} : \mathcal{D} \to \mathcal{D}\\
&w = g_\zeta^{-1} = \frac{w'-\zeta}{1-\zeta^* w'}
\end{aligned}$$

Given a Schur function $\phi \in \mathcal{S}$ with the constraint $\phi(0) = \gamma_1 \in \mathcal{D}$, we can construct the function:

$$\widetilde{\phi}(w) = \frac{1}{w}\frac{\phi(w)-\gamma_1}{1-\gamma_1^*\phi(w)} = \frac{1}{w} g_{\gamma_1}^{-1}\left(\phi(w)\right) \tag{2.10}$$

It can be shown that $\widetilde{\phi}$ is a Schur function. This means that for any Schur function $\widetilde{\phi}(w)$ the Schur function

$$\phi(w) = \frac{w\widetilde{\phi}(w)+\gamma_1}{1+\gamma_1^*\widetilde{\phi}(w)} = g_{\gamma_1}\left(w\widetilde{\phi}(w)\right) \tag{2.11}$$

with $\phi(0) = \gamma_1$ can be constructed. Using the Möbius transformation $h_{Y_1}(z)$, we can go further and construct the function $\theta(z) = \phi \circ h_{Y_1}(z)$ which follows the constraint that $\theta(Y_1) = \gamma_1$:

$$\theta(z) = \frac{\frac{z-Y_1}{z-Y_1^*}\widetilde{\theta}(z) + \gamma_1}{\gamma_1^* \frac{z-Y_1}{z-Y_1^*}\widetilde{\theta}(z) + 1} = g_{\gamma_1}\left(h_{Y_1}(z)\widetilde{\theta}(z)\right) \tag{2.12}$$

Where $\widetilde{\theta}$ is any contractive function. This way we can iteratively construct $\theta_1, \theta_2, ..., \theta_{M+1}$. θ_1 is constructed by $\theta_1 = g_{\lambda_1}(h_{Y_1}(z)\theta_2(z))$. Therefore it satisfies $\theta_1(Y_1) = \lambda_1$. If we want it to also satisfy $\theta_1(Y_\alpha) = \lambda_\alpha$ for $\alpha = 2, ..., M$, we have to make sure that θ_2 satisfies $\theta_2(Y_\alpha) = \lambda_\alpha^{(2)}$ for $\alpha = 2, ..., M$ where

$$\lambda_\alpha^{(2)} = \frac{Y_\alpha - Y_1^*}{Y_\alpha - Y_1} \frac{\lambda_1^{(1)} - \lambda_1^{(1)}}{(\lambda_1^{(1)})^* \lambda_\alpha^{(1)} - 1} \tag{2.13}$$

Similar constraints can be made for $\theta_3, \theta_4, ...$. In the end, only θ_{M+1} remains free to choose and is determined by the Hardy optimization step[2].

To obtain the retarded Green function, we remember that by 2.9, λ_n are the contracted values G_n of the Matsubara Green function. The approximation for the Green function is the inverse Möbius of 2.9 transformation applied to θ_1:

$$G(z) = h_i^{-1}(\theta(z)) \tag{2.14}$$

2.3 PES

Another new approach for the analytic continuation problem is the *PES* method[11]. PES is short for **P**rojection into causal space, pole **E**stimation, and **S**emidefinite relaxation, indicating that the method is a three-step procedure. The PES method is particularly aimed at systems with finite numbers of allowed energy levels leading to discrete energy spectra. To grasp the meaning of these steps, we use that in this case the Green function can be written as:

$$G(z) = \sum_{l=1}^{N_p} \frac{X_l}{z - \lambda_l} \tag{2.15}$$

Here I follow the convention of [11] and write the double sum over the energy levels n, n' to a single sum $\sum_l$ where N_p is the number of energy levels squared. The numerators $\frac{1}{Z}\langle n|c|n'\rangle\langle n'|c^\dagger|n\rangle \cdot (e^{-\beta E_n} + e^{-\beta E_{n'}})$ in 1.15 are absorbed into X_l and the energy differences $E_n - E_{n'}$ are absorbed into λ_i. Notice that all X_l are nonnegative. Because every discrete-energy Green function is of this form, one can define the *causal space* which contains every possible $G(z)$:

$$\mathcal{S}_F = \left\{ G \;\middle|\; G(z) = \sum_{l=1}^{N_p} \frac{X_l}{z - \lambda_l}, \text{ for } \lambda_l \in \mathbb{R} \text{ and } X_l \in \mathbb{R}_+ \right\} \tag{2.16}$$

[2] For more details on how θ_{M+1} is chosen, see Section 2.2.5 in [5].

The subscript F denotes that these Green functions are for fermionic systems. The causal space for bosonic systems can be defined in a similar way.
For simplicity, only the single-orbital case is discussed here. In the general fermionic case, $G(z)$ would become a matrix $\mathbb{G}(z)$ whose components $\mathbb{G}_{ij}$ correspond to the orbital in which a state is annihilated (c_i) or constructed $(c_j^\dagger)$. The constraints for $\mathbb{X}_l$ which are the generalizations of the X_l are different, namely that they are rank-1 and positive semidefinite.

2.3.1 Projection

The Green function with respect to the Matsubara frequencies $G(i\omega_n) \equiv G_n$ is often obtained numerically. For some of these techniques, especially for Monte-Carlo simulations, the data contains unphysical noise. It is more desirable to start with data that corresponds to a possible physical system, i.e. data that lies in the causal space $\mathcal{S}_F$. To achieve this, we project the data into the causal space. We can do this by choosing a set of equidistant points x_m, $m = 0, ..., M$ around 0 on the real axis. Our goal is to find a set $\{P_m \in \mathbb{R}_+, m = 0, .., M| \sum_{m=0}^{M} P_m = 1\}$ such that the error

$$\mathcal{E}_{\text{proj}}(P_m) = \sum_{n=1}^{N_w} \left\| G_n - \sum_{m=0}^{M} \frac{P_m}{i\omega_n - x_m} \right\|^2 \tag{2.17}$$

is minimal. Here, $\|\cdot|$ indicates the Frobenius norm. This convex optimization problem can in practice be solved by using software packages like Convex.jl. The projected Matsubara data G_n^{proj} is now:

$$G_n^{\text{proj}} = \sum_{m=0}^{M} \frac{P_m}{i\omega_n - x_m} \tag{2.18}$$

This initial step is independent of the remaining steps of the procedure, but one finds that it improves the quality of the final result. It can also be used as a preprocessing step to improve other analytic continuations.

2.3.2 Pole estimation

One could argue that we are done after this first step because it yields an expression 2.18 which already is an analytic continuation (we could simply replace $i\omega_n$ with $\omega + i\eta$). However, in practice, the accuracy which is needed for the pole locations is much higher than the distance between the points x_n. To get a more precise estimation for the poles the Antoulas-Anderson algorithm (AAA) is used. In A an explanation of how it works is given. It provides a rational function that approximates the input data. The zeros of its denominator can be used to get a better estimation of the pole locations.

2.3.3 Semidefinite relaxation

In the last step, the final sets $\{X_l\}$ and $\{\lambda_l\}$ are determined. The step is called semidefinite relaxation because, in the multi-orbital case, $\mathbb{X}_l$ are semidefinite matrices. This constraint is then dropped in this step.
Of course, we want to choose them such that the resulting Green function is as close as possible to our projected data G_n^{proj}, i.e. the error

$$\text{Err}(\{\lambda_l\}_{l=1}^{N_p}, \{X_l\}_{l=1}^{N_p}) = \left(\sum_{n=1}^{N} \left\| G_n - \sum_{l=1}^{N_p} \frac{X_l}{i\omega_n - \lambda_l} \right\|^2 \right)^{1/2}$$

should be minimal. When the poles $\{\lambda_l\}$ are fixed this becomes a convex optimization problem which can be solved very efficiently using Convex.jl and SCS.jl. The optimization of poles, however, is nonconvex.
To tackle this problem a bilevel optimization approach is used. We define the error function for a set of poles $\{\lambda_l\}$ where the corresponding optimal $\{X_l\}$ are found by convex optimization:

$$\mathcal{E}(\{\lambda_l\}_{l=1}^{N_p}) = \min_{X_l \geq 0} \text{Err}(\{\lambda_l\}_{l=1}^{N_p}, \{X_l\}_{l=1}^{N_p})$$

For the initial poles, we use the data from the second step. Since $\mathcal{E}$ as well as X_l are functions of $\{X_l\}$, we can find an expression for the partial derivative:

$$\partial_m \mathcal{E} = \frac{\partial}{\partial \lambda_m} \text{Err} + \sum_{l=1}^{N_p} \frac{\partial \text{Err}}{\partial (X_l)} \bigg|_{X_l^{opt}} \cdot \frac{\partial X_l^{opt}}{\partial \lambda_m}$$

To minimize $\mathcal{E}(\{\lambda_l\}_{l=1}^{N_p})$ we can now use a gradient-based optimization solver that also includes the information about the gradient into the calculation.
Note that 2.15 only applies to finite energy systems. For continuous energy systems, the expression would become an integral over energies as in 1.25. In principle, PES could also work for continuous energy systems if the number of X_l is increased so that 2.15 approaches an integral. Therefore in the next chapter, PES is also applied to the data for a continuous energy system.

Chapter 3

Results

Before showing the results of the calculations, I want to give a list of the questions I try to answer.

- Can PES also be applied to Matsubara Green functions that correspond to systems with continuous energy spectra?
- Can the Projection step improve the quality of other analytic continuation methods?
- How does the Nevanlinna method perform compared to Padé approximation?
- Can the AAA algorithm lead to a more efficient or accurate analytic continuation than previous rational approximation techniques?
- How robust are all of the mentioned analytic continuations to noise in the input data?

For all of the tests that are shown below, the spectral functions that are calculated by analytic continuation of the Matsubara function are compared with the (numerically) exact spectral functions.

3.1 Rational approximation

First, we will compare Padé approximation with rational approximation using the AAA algorithm[1].

For AAA the implementation in the 'baryrat' python package is used [12]. For Padé approximation, the 'ana_cont' python package is used [13].

The results for the spectral function of the single impurity Anderson model are shown in Fig. 3.1. Both approaches yield good results. The errors of the exact spectral function

[1] Here, I call the algorithm that is explained in 2.1.1 Padé approximation because it is the algorithm that is usually referred to by this term in this context. Strictly speaking, a Padé approximation is just the best rational approximation for a given function. Since AAA is also using rational functions, it could also be called so.

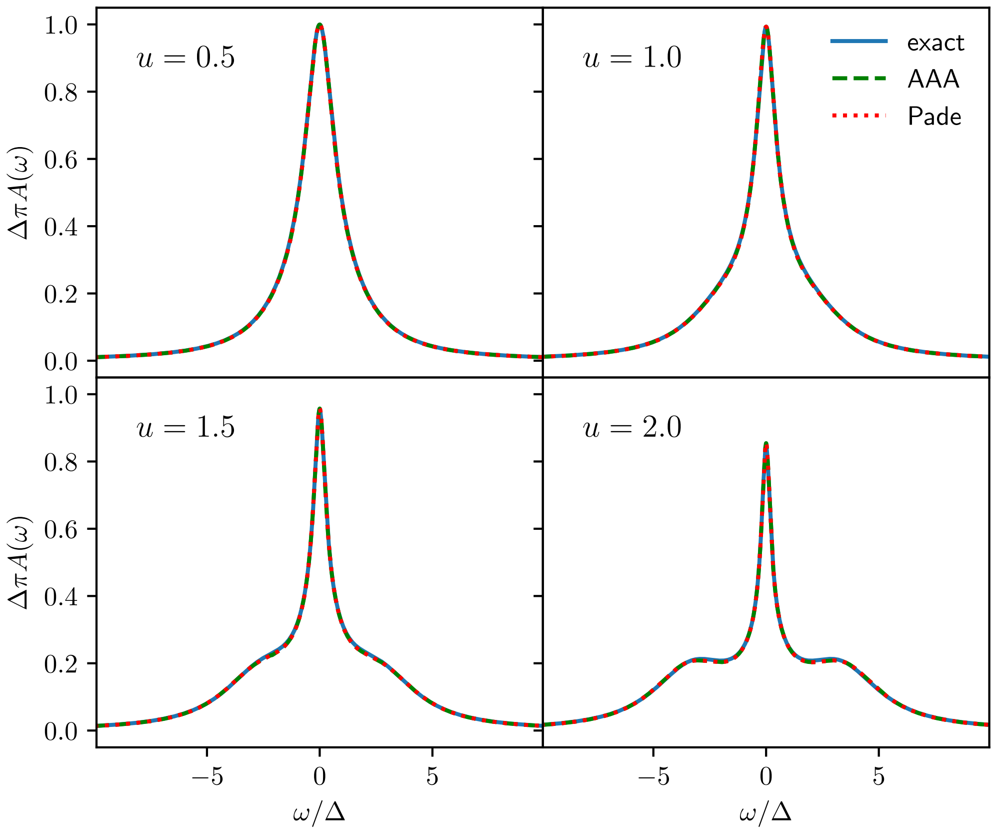

Figure 3.1: The numerically exact spectral function from NRG (blue), as well as the estimation by Padé approximation (red) and AAA algorithm (green), is shown for four different values of U. The spectral function is multiplied with π times the hybridization width Δ. u indicates the dimensionless interaction strength and is related to the U in 1.31 by $u = \frac{U}{\pi\Delta}$.

can hardly be seen. Therefore, in Fig. 3.2 the deviation from the exact spectral function is shown. Both methods yield roughly the same approximation.

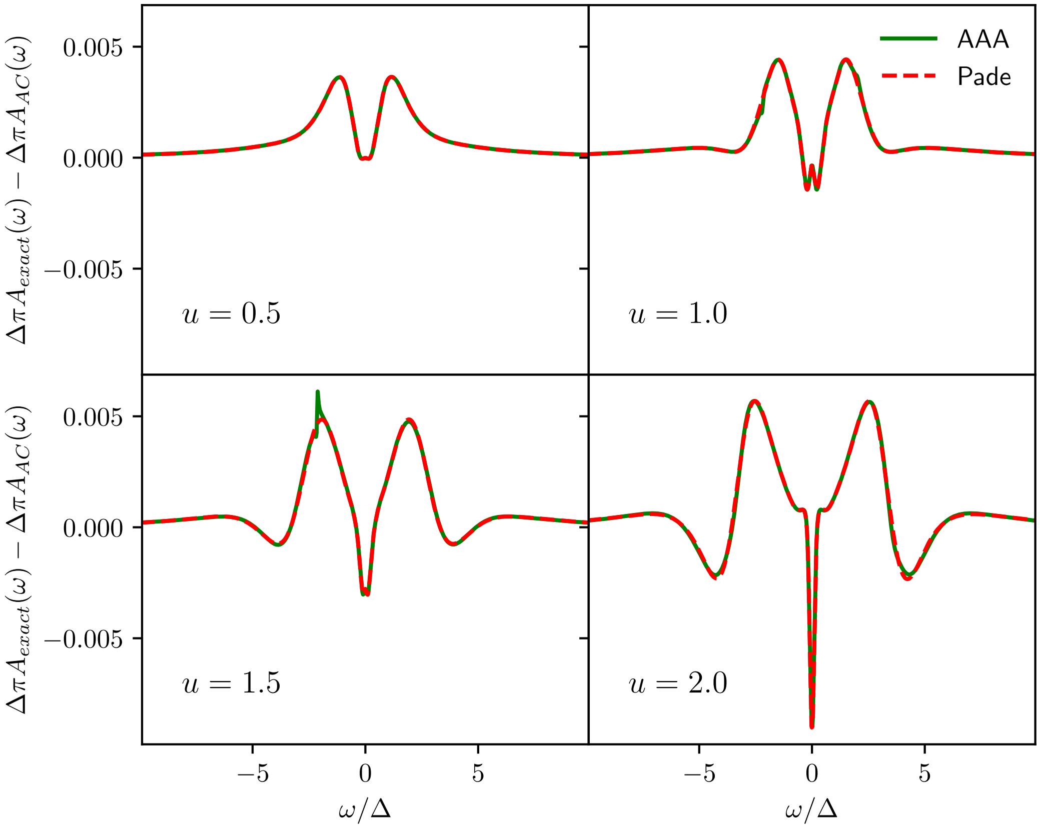

Figure 3.2: The error of the analytic continuation which is shown in 3.1

To see a difference between the two approaches, we need to consider a Matsubara function that corresponds to a more complicated spectral function. This is done in Fig. 3.3. The function shown does not correspond to a particular physical system. It is composed of Gauss functions such that it contains both very fine and broad features. Now, the AAA algorithm performs much better although the positivity constraint is violated slightly. For Padé, the first thirty Matsubara frequencies were chosen. The analytic continuation could be enhanced by increasing that number. However, this would also increase calculation time. Already for the data shown, Padé took much longer to compute in comparison to AAA. The reason for this is that AAA chooses the Matsubara points that are used for interpolation by itself while still making sure that the resulting function approximates all points well.

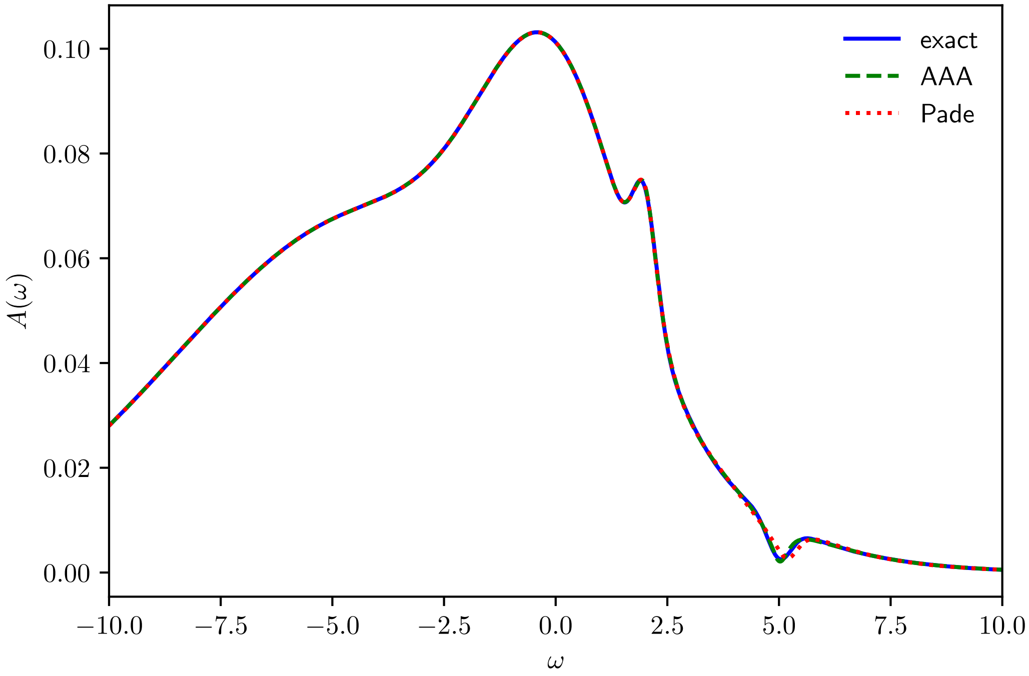

Figure 3.3: AAA (green) and Padé (red) analytic continuation for data corresponding to an arbitrary spectral function (blue). The spectral function contains both very fine and broad features.

3.2 Nevanlinna

Next, we will see how well the Nevanlinna analytic continuation performs on the SIAM data.
For the calculations, I used the Nevanlinna.jl package for Julia [5]. In general, the code package does not prove to be very reliable, as several problems occurred to me while testing. Depending on the data for the Matsubara function, the Hardy optimization step sometimes did not work at all. In other cases, the Hardy optimization seems to reduce the quality of the analytic continuation instead of increasing it. Here, it is left out for that reason. Also, in some cases, using 128-bit precision lead to worse results than double float precision which is unintuitive because higher precision should make the algorithm more numerically stable. For the SIAM, double precision is used. The results are shown in Fig. 3.4. Nevanlinna gives a reasonable approximation of the spectral function. However, compared to rational function approximatiosn, is it less precise.

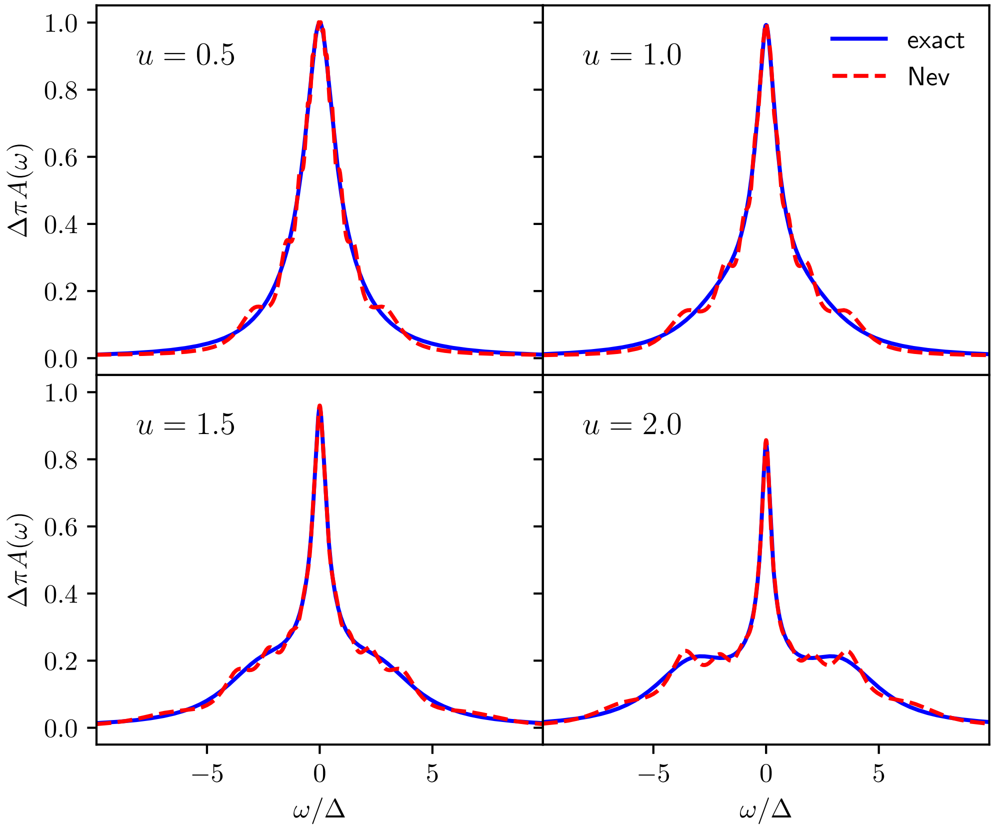

Figure 3.4: The exact spectral function (blue) and the spectral function obtained by Nevanlinna analytic continuation (red) is shown for four different values of u.

3.3 PES

In PES, the final Green function will be in the representation shown in equation 2.15. We can see that this representation leads to a sum of Lorentz peaks in the resulting spectral function:

$$A(\omega) = -\frac{1}{\pi}\mathrm{Im}G(\omega + 0^+) = -\frac{1}{\pi}\mathrm{Im}\sum_{l=1}^{N_p}\frac{X_l}{\omega - \lambda_l}$$
$$= -\frac{1}{\pi}\sum_{l=1}^{N_p}\frac{X_l \cdot \mathrm{Im}\lambda_l}{(\omega - \mathrm{Re}\lambda_l)^2 + (\mathrm{Im}\lambda_l)^2} \tag{3.1}$$

PES was designed to work for systems with discrete energy levels. Here, I test if it can also be applied to continuous energy systems. In principle this could work., because representing a spectral function as a sum of Lorentz functions is possible. This is illustrated in Fig. 3.5.

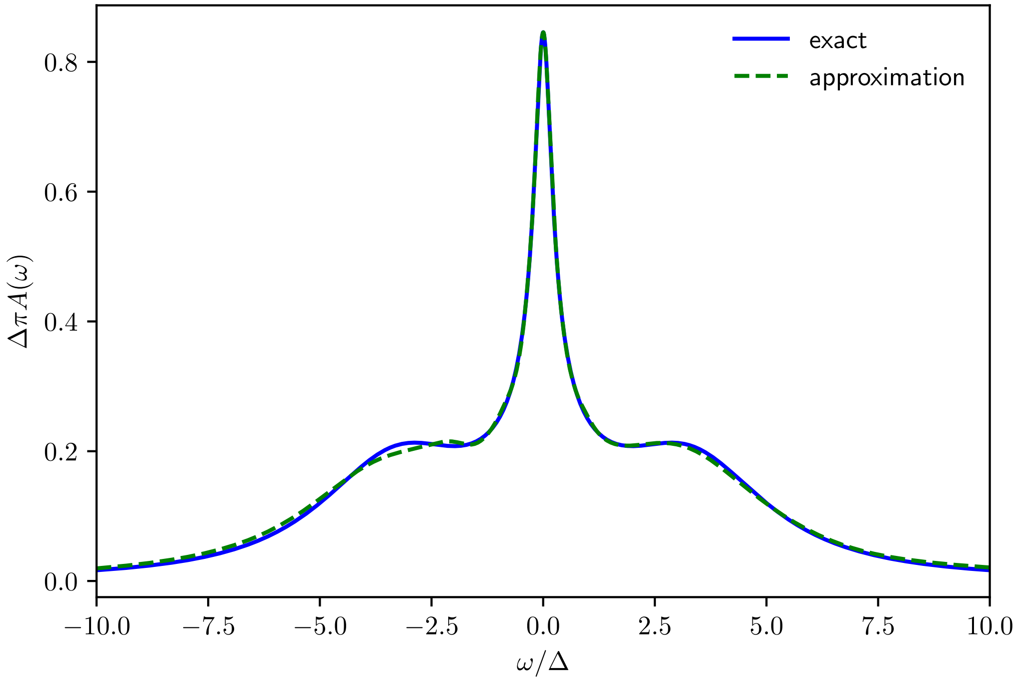

Figure 3.5: The exact spectral function of the SIAM for $u = 1.5$ is shown (blue) as well as an approximation (blue). The approximation is a sum of 99 single Lorentz peaks. The approximation was done in the following way: Using AAA, the set of poles for the spectral function was determined. From that, the spectral function can be created analogously to 3.1 where to each pole a weight is assigned. The weights here are chosen using the Optim.jl optimization package to best fit the exact function.

I wrote an own implementation of PES in Julia following the existing software for Matlab [11]. For the Convex optimization, I used the packages Convex.jl and SCS.jl. For non-discrete spectral function, the projection step does not work and leads to awkward results. This is not surprising, because the step forces the data for the Matsubara function to follow the representation given in 2.15 which does not apply to systems with continuous energy levels. Therefore, in the discussion here, it is left out.
In Fig. 3.6 we can see the result that the PES analytic continuation yields for the SIAM data. Each single lorentz function, which together make up the approximation, is also depicted. This representation fails to give a good approximation, especially for the broad parts of the curve. Thus, it can be concluded that the PES method is not suited for the analytic continuation in systems with continuous energy levels.

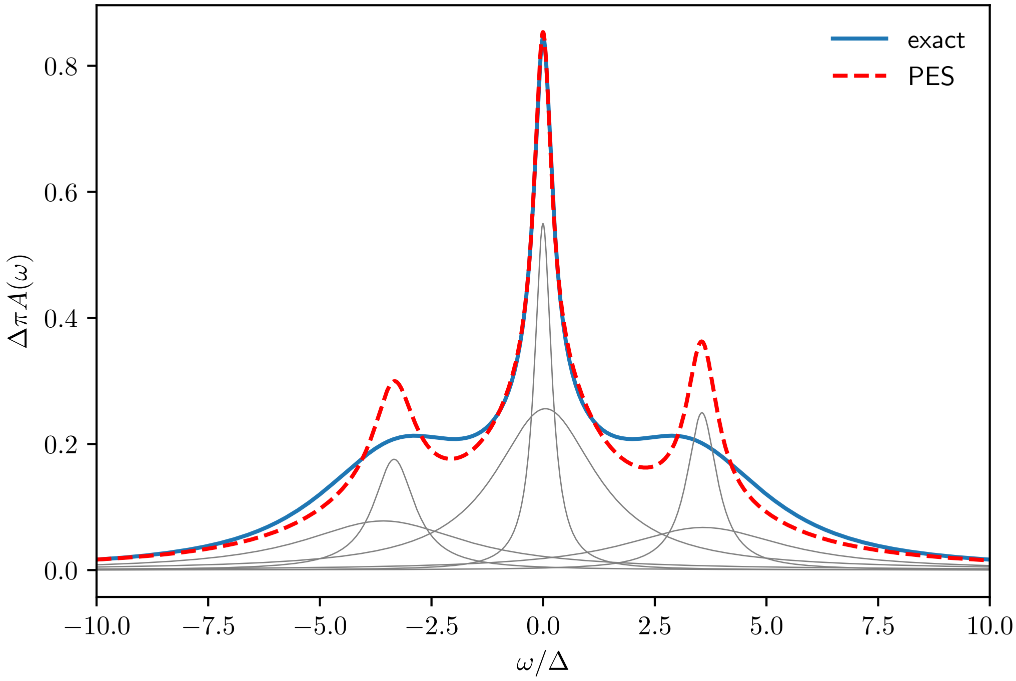

Figure 3.6: PES for the NRG spectral function. Each thin line represents a lorentz function. Together they make up the approximation. Lorentz function whose weights are very small are not shown.

3.4 Noisy data

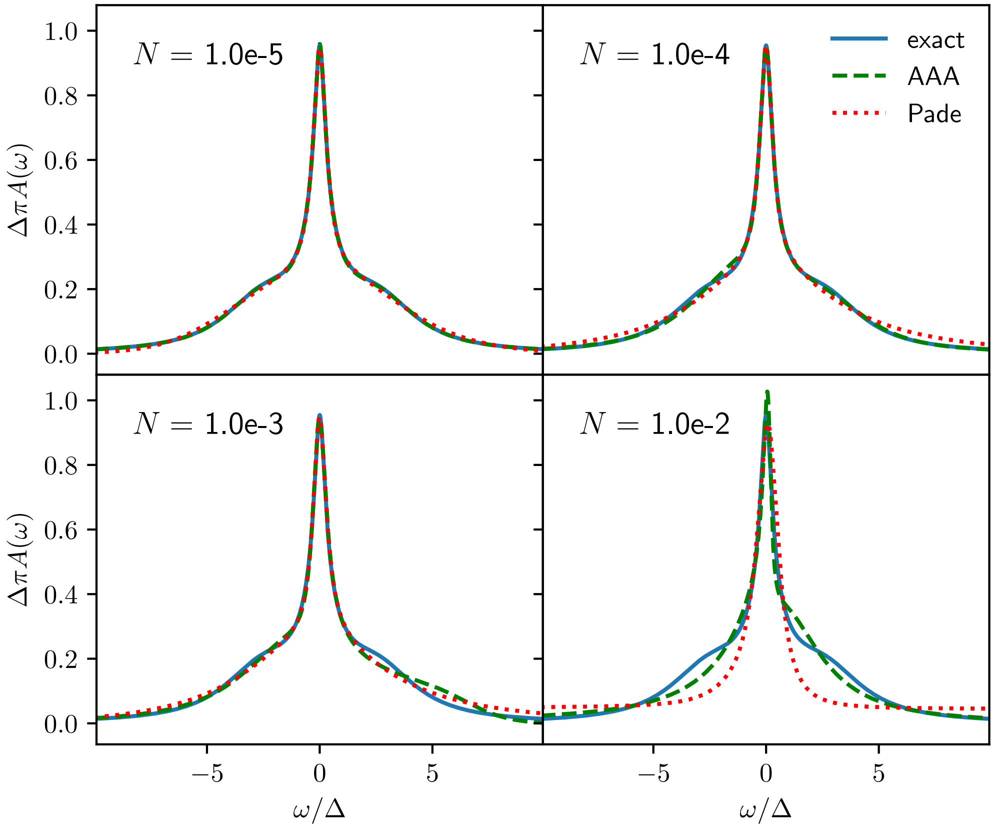

Figure 3.7: Analytic continuation by rational approximation is shown for four different levels of noise ($u = 1.5$).

We will now look at what happens when random noise is artificially added to the Matsubara Green function. This is of practical importance because many calculations for the Matsubara Green function are done by Monte Carlo simulations which leads to at least some noise in the result. To simulate the noise that occurs in numerical calculations, to each data point, a random number is added. These random numbers are samples from a Gauss distribution where the variance is equal to the absolute value of the data point times the noise level N.
The rational approximations prove to be very robust to noise. This can be seen in Fig. 3.4, where high levels of noise are added to the data.
Nevanlinna fails when the data contains strong noise. The reason for this is that a holomorphic and positive function that interpolates all Matsubara points does not exist [5].

The discussion on how PES performs on noisy NRG data is left out here because we already concluded that PES is not suited for this type of system.

3.5 Discrete spectral functions

Finally, we also want to test the discussed methods for systems with discrete energy levels. For instance, this could be a single atom or molecule.
To do this, we create an arbitrary discrete spectral function. We then calculate the corresponding Green function for a set of Matsubara frequencies using 1.25.

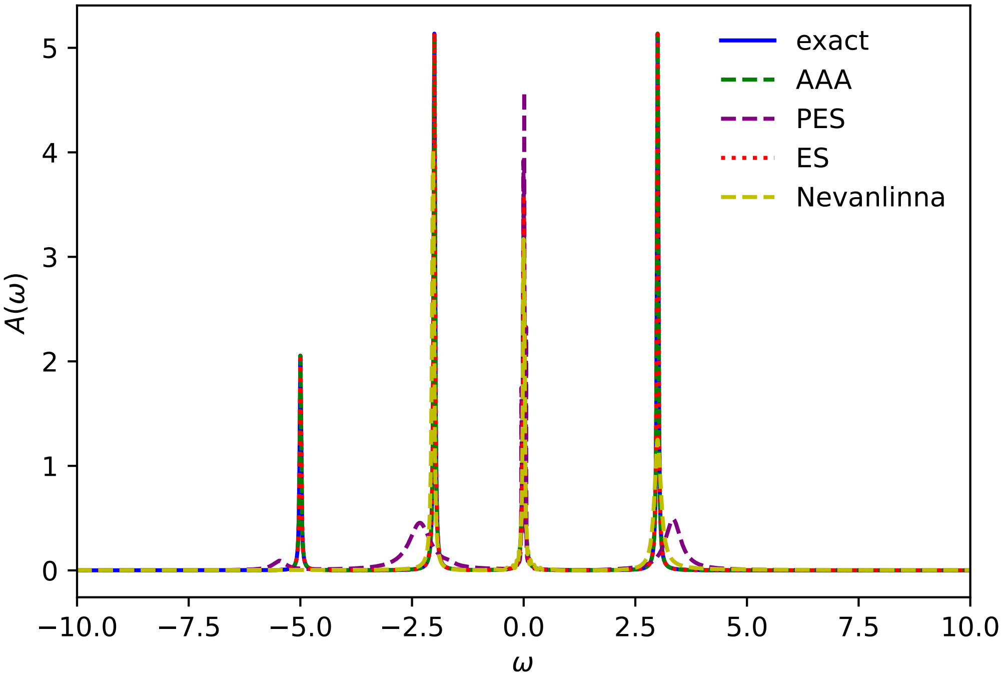

Figure 3.8: The analytic continuation done by PES (green), PES without projection (red) AAA (purple), and Nevanlinna (yellow) of a discrete energy system is shown.

In Fig. 3.8 the results for AAA, Nevanlinna, and PES are shown. In addition to PES, the results that are obtained without the Projection step are also shown. PES without Projection and AAA yield the best results. The position as well as the height of the four peaks are captured correctly by both methods. PES with Projection gets the position of the peaks only approximately right while failing totally at their height. Finally, Nevanlinna only gets three of the four positions right while also failing at their height.
Again, we can artificially add noise to the Matsubara Green function in the same way as done in 3.4.

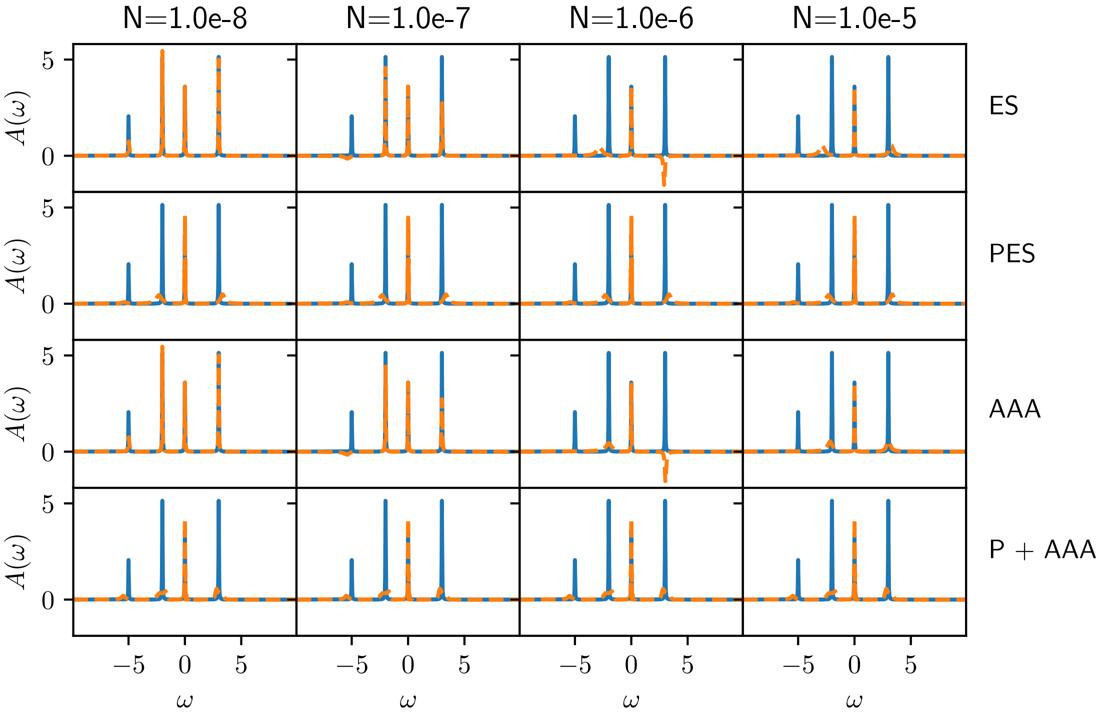

Figure 3.9: The influence of noise on the analytic continuation of a discrete energy system is shown for PES, PES (without projection), AAA algorithm, and AAA algorithm in addition to the projection step.

In Fig. 3.9 the results for that can be seen. Nevanlinna is left out here because it leads to results that are not useful at all. Instead, AAA is shown when the Projection step of PES is applied to the Matsubara data before the analytic continuation to investigate the claim made in [11] that the Projection step can also enhance the analytic continuation of noisy input data in other methods.

In all cases, the noise strongly affects the quality of the analytic continuation. When the Projection step is left out, the spectral function has negative values for some frequencies which is unphysical. The Projection step is able to restrict the outcome to only a positive function when the remaining two steps of PES and the AAA algorithm are used. The best results are obtained by the PES method because it best respects the shape of the discrete spectral function. Interestingly, all the spectral functions, where the data was projected, look very similar. The reason for this is that the Projection step changes the data for the Matusbara function to correspond exactly to a function in the causal space $\mathcal{S}_F$ defined in 2.3. However as seen in Fig. 3.8, if there is no noise the data is mapped function in $\mathcal{S}_F$ that is not the "true" Green function. I assume that the reason for this is that the grid which is created as explained in 2.3.1 is too coarse.

Chapter 4

Conclusion and outlook

4.1 Conclusion

The data presented in Chap. 3 provides answers to the questions posed at the beginning of the chapter. The key findings can be summarised as follows:

- The PES method is not suitable for systems with continuous energy spectra. Although PES uses a representation that can lead to continuous spectral functions, in practice, the method does not give appropriate results for most of them. Thus, the use of PES is restricted to systems with a finite number of energy states.

- The Projection step can not be used to improve the quality of other analytic continuation techniques for continuous energy systems. This fact is not too surprising since the Projection step forces the data into the representation in 2.15 which does not hold for this kind of system.
  Even further and in contrast to the claims made in [11], the data shown in 3.9 suggests that in the discrete energy case, the Projection step reduces the quality of the remaining two steps of the PES method when the noise is weak. Only in certain cases, when strong noise is added to the data, the Projection step leads to better results.

- The Nevanlinna method leads to reasonable results for the spectral function of the SIAM. However, a rational approximation of data is both more efficient and more precise.

- As an alternative to Padé, the AAA algorithm can be used for analytic continuation using rational functions. The most important difference in practice is that in Padé approximation the Matsubara frequencies which are used for interpolation have to be chosen manually. The quality of the results strongly depends on that choice. Generally speaking, interpolating more Matsubara frequencies leads to better results but also longer calculations. Simply choosing all available frequencies is usually not an option. The AAA algorithm does not have that issue. The algorithm works by

choosing the optimal support points on its own. For simple spectral functions, both methods yield results that are equally good. For more complicated spectral functions, when more Matsubara frequencies are needed for a precise estimate, the AAA algorithm is superior.
Also, it is worth mentioning that the AAA algorithm is extremely easy to use. Implementations can easily be found in Julia or Python packages. Most of the code needed for the calculation consisted of a few lines and ran in a fraction of a second.

- Nevanlinna fails at noisy data because a function that interpolates through all Matsubara points can not be found. Both Padé and AAA prove to be resistant to noise. PES also gives reasonable results even for strong noise. The Projection step is able to get adequate results from data that otherwise would yield total nonsense.

Method	Continuous	Discrete	Continuous + Noise	Discrete + Noise	Spectral function is always positive
Padé	+		o		✗
AAA	++	++	+	o	✗
Nevanlinna	+	−	☠	☠	✓
ES	−−	++	☠	o	✗
PES	☠	o	☠	+	✓

Table 4.1: A general overview over the performance of the tested methods is given. They are ranked from very good (++) over okay (o) to very bad (−−). ☠ means that the method can not be used for the specific case at all. Padé was not tested for the discrete spectra but is expected to perform similar to AAA.

4.2 Outlook

Out of all the methods that were tested, AAA showed to be the most reliable method for analytic continuation. In addition, it is very easy and straightforward to use. Also, packages containing ready to use implementations are available publicly for Python and Julia [12][14]. In short, AAA showed to be an improved Padé approximation.
However, some of the problems that are known for Padé continue to occur in AAA. Most strikingly, for data that contains strong noise, the final spectral function does not necessarily obey the positivity constraint (see Figure 3.9). A question for future research could be to investigate whether AAA could be modified in a way to ensure that this constraint is fulfilled. Maybe, this could be achieved by preprocessing steps similar to PES's projection or by modifying the algorithm itself.

Appendix A

AAA algorithm

The *AAA algorithm* is used to approximate a function $f(z)$ that is known on a set of points $f(z_i) = f_i$, $i = 1, ...M$ by using a rational function. It uses the *barycentic representation* of rational functions:

$$r(z) = \frac{n(z)}{d(z)} = \frac{\sum_{j=1}^{M} \frac{w_j f_j}{z - z_j}}{\sum_{j=1}^{M} \frac{w_j}{z - z_j}} \tag{A.1}$$

where $w_1, ..., w_M$ are weights. Note that for any choice of $w_1, ..., w_M$, $w_i \neq 0$, $r(z)$ satisfies the constraints $f(z_i) = f_i$. However, in practice, it is usually not necessary to include all support points z_i and function values f_i in A.1 because a much smaller number of points can obtain a good approximation for $f(z)$. The algorithm decides which z_i are chosen and calculates the optimal choice for the weights w_i.

The algorithm works iteratively. Let Z be the set of all support points. At each step m a new support point z_m from the set of remaining support points $Z^{(m-1)} = Z \backslash \{z_1, ..., z_{m-1}\}$ is chosen. It is chosen when the difference between the current approximation $r(z)$ and $f(z)$ has the largest absolute value. At step m a new point z_m is carefully chosen from the set of support points that have not been used $Z^{(m-1)} = Z \backslash \{z_1, ..., z_m\}$. The weights $w_1, ..., w_m$ are then determined by solving the linear least-square problem over the remaining points $Z^{(m)}$:

$$\min_{\|w\|_2 = 1} \|fd - n\|_2 \tag{A.2}$$

We write the support points $Z^{(m)}$ and their corresponding function values $F^{(m)} = f(Z^{(m)})$ as column vectors:

$$Z^{(m)} = (Z_1^{(m)}, ..., Z_{M-m}^{(m)})^T$$
$$F^{(m)} = (F_1^{(m)}, ..., F_{M-m}^{(m)})^T$$

A.2 can be written in matrix form:

$$\min_{\|w\|_2 = 1} \|A^{(m)} w\|_2 \tag{A.3}$$

where A is a $(M-m)\times m$-matrix:

$$A = \begin{pmatrix} \frac{F_1^{(m)}-f_1}{Z_1^{(m)}-z_1} & \cdots & \frac{F_1^{(m)}-f_m}{Z_1^{(m)}-z_m} \\ \vdots & \ddots & \vdots \\ \frac{F_{M-m}^{(m)}-f_1}{Z_{M-m}^{(m)}-z_1} & \cdots & \frac{F_{M-m}^{(m)}-f_m}{Z_{M-m}^{(m)}-z_m} \end{pmatrix} \tag{A.4}$$

A.3 can be solved using a singular value decomposition of $A = U\Sigma V^\dagger$. U is a unitary matrix. Σ is a diagonal matrix containing the singular values of A. $V^\dagger$ is the complex conjugate of the unitary matrix V. The singular values are non-negative real numbers. The singular values are ordered by size, i.e. $\sigma_{11} \geq \sigma_{22} \geq \ldots$. For any matrix at least one singular value decomposition exists and Σ is always unique. The optimal w is then given by the last column vector of V corresponding to the smallest singular value.

The algorithm terminates as soon as the error in A.2 is smaller than a given tolerance which is usually set to 10^{-13} as the default value in most implementations. The power of the AAA algorithm is that usually, the number of support points that is sufficient to get a good approximation for all points is much smaller than the number of total constraints M.

Bibliography

[1] J. D. Jackson, *Classical electrodynamics.* Wiley, 3. edition ed., 1999.

[2] M. body quantum theory in condensed matter physics and H. Bruus, *Many-body quantum theory in condensed matter physics.* Oxford graduate texts, Oxford Univ. Press, reprint. ed., 2007.

[3] A. L. Fetter, *Quantum theory of many-particle systems.* Mineola, N.Y.: Dover Publ., [corr. repr. of the 7. print of the work first publ. by the mcgraw-hill book comp., new york, in 1971] ed., 2003.

[4] G. Baym and N. D. Mermin, "Determination of Thermodynamic Green's Functions," *Journal of Mathematical Physics*, vol. 2, pp. 232–234, Dec. 2004.

[5] K. Nogaki, J. Fei, E. Gull, and H. Shinaoka, "Nevanlinna.jl: A Julia implementation of Nevanlinna analytic continuation," Feb. 2023. https://arxiv.org/abs/2302.10476v1.

[6] H. Shinaoka, J. Otsuki, M. Ohzeki, and K. Yoshimi, "Compressing Green's function using intermediate representation between imaginary-time and real-frequency domains," *Physical Review B*, vol. 96, p. 035147, July 2017.

[7] R. Bulla, T. A. Costi, and T. Pruschke, "Numerical renormalization group method for quantum impurity systems," *Reviews of Modern Physics*, vol. 80, pp. 395–450, Apr. 2008.

[8] H. J. Vidberg and J. W. Serene, "Solving the Eliashberg equations by means ofN-point Padé approximants," *Journal of Low Temperature Physics*, vol. 29, pp. 179–192, Nov. 1977.

[9] Y. Nakatsukasa, O. Sète, and L. N. Trefethen, "The AAA algorithm for rational approximation," *SIAM Journal on Scientific Computing*, vol. 40, pp. A1494–A1522, Jan. 2018.

[10] L. N. Trefethen, "Numerical analytic continuation," *Japan Journal of Industrial and Applied Mathematics*, June 2023.

[11] Z. Huang, E. Gull, and L. Lin, “Robust analytic continuation of Green’s functions via projection, pole estimation, and semidefinite relaxation,” *Physical Review B*, vol. 107, p. 075151, Feb. 2023. arXiv:2210.04187 [cond-mat, physics:physics].

[12] Clemens, “Barycentric rational approximation,” May 2023. https://github.com/c-f-h/baryrat.

[13] J. Kaufmann, “ana_cont: Python package for analytic continuation,” July 2023. https://github.com/josefkaufmann/ana_cont.

[14] D. MacMillen, “BaryRational,” May 2023. original-date: 2021-01-19T08:00:17Z.

Selbständigkeitserklärung

Hiermit erkläre ich, die vorliegende Arbeit selbständig verfasst und keine anderen als die angegebenen Quellen und Hilfsmittel benutzt zu haben.

München, 24. Juli 2023

Philipp Kaufmann